Cite as: L. Rougé *et al.*, *Science* 10.1126/science.aaz9356 (2020).

Structure of CD20 in complex with the therapeutic monoclonal antibody rituximab

Lionel Rougé[1], Nancy Chiang[2], Micah Steffek[3], Christine Kugel[4], Tristan I. Croll[5], Christine Tam[4], Alberto Estevez[1], Christopher P. Arthur[1], Christopher M. Koth[1], Claudio Ciferri[1], Edward Kraft[4], Jian Payandeh[1,2]*, Gerald Nakamura[2]*, James T. Koerber[2]*, Alexis Rohou[1]*

[1]Department of Structural Biology, Genentech Inc., South San Francisco, CA 94080, USA. [2]Department of Antibody Engineering, Genentech Inc., South San Francisco, CA 94080, USA. [3]Department of Biochemical and Cellular Pharmacology, Genentech Inc., South San Francisco, CA 94080, USA. [4]Department of Biomolecular Resources, Genentech Inc., South San Francisco, CA 94080, USA. [5]Cambridge Institute for Medical Research, University of Cambridge, Keith Peters Building, Cambridge CB2 0XY, UK.

*Corresponding author. Email: rohou.alexis@gene.com (A.R.); koerber.james@gene.com (J.T.K.); nakamura.gerald@gene.com (G.N.); payandeh.jian@gene.com (J.P.)

Cluster of Differentiation 20 (CD20) is a B cell membrane protein that is targeted by monoclonal antibodies for the treatment of malignancies and auto-immune disorders, but whose structure and function are unknown. Rituximab (RTX) has been in clinical use for two decades, but how it activates complement to kill B cells remains poorly understood. We obtained a structure of CD20 in complex with RTX, revealing CD20 as a compact double-barrel dimer bound by two RTX antigen-binding fragments (Fabs), each of which engages a composite epitope and an extensive homotypic Fab:Fab interface. Our data suggest that RTX crosslinks CD20 into circular assemblies and lead to a structural model for complement recruitment. Our results further highlight the potential relevance of homotypic Fab:Fab interactions in targeting oligomeric cell-surface markers.

The integral membrane protein Cluster of Differentiation 20 (CD20) is a B cell-specific marker and a clinically-validated therapeutic target for B cell malignancies and auto-immune conditions (*1*). It is ubiquitously expressed on circulating B cells (*2*) and is predicted to have four transmembrane (TM) helices with two extracellular loops, ECL1 and ECL2, the second of which is much longer and contains a disulfide bond (fig. S1A). These topological features are conserved among a group of membrane proteins called MS4A (membrane-spanning 4-domain family, subfamily A), which includes 18 proteins identified through similarities between their amino acid sequences but whose biological functions are mostly unknown (*3*). Aside from structures of short ECL2 peptide segments from CD20 (*4*, *5*), there exists no high-resolution structural data on any MS4A family member beyond predictions of secondary structure and membrane topology. While CD20 is the best-studied member of the family, even its oligomeric state is poorly understood: available evidence suggests it associates into homo-oligomers and complexes with other proteins (*6*–*8*). In addition, the function of CD20 remains an area of active debate. Early work suggested that CD20 functions as an ion channel because overexpression and knockout of CD20 can increase or decrease Ca^{2+} conductance in B cells, respectively (*6*, *9*). However, more recent work showed that $CD20^{+}$ B cells lacking the B cell receptor (BCR) are unable to initiate calcium signaling, suggesting that CD20 indirectly regulates calcium release downstream from the BCR (*10*).

CD20-targeted therapies revolutionized the treatment of B cell malignancies and auto-immune disorders, starting with the monoclonal antibody (mAb) rituximab (RTX; Rituxan®), which was the first approved therapeutic mAb for cancer and continues to be the benchmark for second- and third-generation mAbs (*1*, *11*). Another anti-CD20 mAb, ocrelizumab (OCR; Ocrevus®), is now used in the treatment of multiple sclerosis (*12*). While all anti-CD20 mAbs act by depleting B cells, they employ at least four distinct mechanisms (*13*): direct cell death, FcR effector functions through antibody-dependent cellular cytotoxicity (ADCC) and phagocytosis (ADCP), and complement-dependent cytotoxicity (CDC). Each therapeutic antibody varies in its ability to trigger each pathway and there is no molecular-level understanding of why this is the case, but these distinct functional effects have been useful in categorizing anti-CD20 mAbs into either type I or type II (*1*, *13*). Rituximab is the prototypical type I mAb, characterized by high CDC activity and the ability to cluster CD20 into lipid rafts (*11*, *14*). Other type I mAbs include OCR and ofatumumab [OFA; (*15*)]. Type II mAbs such as obinutuzumab (OBZ; Gazyva®) and tositumomab (B1; Bexxar®) exhibit low CDC activity, lack the ability to localize CD20 into lipid rafts, but induce higher levels of direct cell death (*16*).

These broad categorizations do not explain how CD20:mAb binding and mAb features lead to different modes of action. One hint at a possible molecular underpinning for these differences is that twice as many type I mAbs bind the surfaces of $CD20^{+}$ cells as type II mAbs (*17*), suggesting that CD20:mAb binding stoichiometry plays a role, though it is

not clear how such strict stoichiometry might arise. Adding to this mystery, some type II and type I mAbs (*e.g.* OBZ and RTX) have overlapping epitopes centered around the ^{170}ANPSE^{174} motif of ECL2, while at least one type I mAb (OFA) has a completely separate, non-overlapping epitope involving ECL1 and another part of ECL2 (*13*). Thus, the location of the epitope on CD20 cannot be the sole determinant of mAb stoichiometry or of therapeutic mode of action. How do antibodies with virtually identical epitope sequences centered on ^{170}ANPSE^{174} bind with different stoichiometries and trigger remarkably different responses? One hint comes from epitope fine-mapping studies showing that residue Asn176 of ECL2 is involved in OBZ binding, but not RTX binding, and that OBZ binds to ECL2 peptides (but not CD20^{+} cells) with higher affinity than RTX (*5*); another hint comes from X-ray crystallographic structures of peptide-bound antigen-binding fragments (Fabs) of RTX, OCR and OBZ, in which RTX and OCR approach the ECL2 epitope at a similar angle, tilted approximately 70° away from the angle at which OBZ approaches the same peptide (*4*, *5*, *18*, *19*). However, in the absence of a structure of full-length CD20 or of a MS4A homolog, it is difficult to speculate how such differences in binding geometry might impact overall binding stoichiometry and dictate therapeutic mode of action.

Results

CD20 forms dimers bound by two RTX Fabs

To facilitate biophysical and structural analyses, we produced human CD20 recombinantly in insect cells and optimized the construct for increased expression (fig. S1A). Following solubilization and purification in the mild detergent glyco-diosgenin (GDN), CD20 was found to be further stabilized by cholesterol hemisuccinate (CHS; fig. S2). Analyzed in GDN-CHS buffer, size exclusion chromatography with multi-angle light scattering (SEC-MALS) indicated that purified CD20 forms stable complexes in 2:2 stoichiometry with RTX Fabs, and 2:1 stoichiometry with OBZ Fabs (fig. S1, C to E, and table S1). Fab binding to purified CD20 was subsequently evaluated using biolayer interferometry (BLI; Fig. 1A) and surface plasmon resonance (SPR; table S2) revealing sensorgrams consistent with a 2-state 2:2 binding of RTX (K_D = 21.4 nM, SPR), and with 2:1 binding of OBZ Fab (K_D = 58.8 nM, SPR). Imaging the resulting CD20:Fab complexes by negative-stain electron microscopy (nsEM) showed that each CD20 particle is bound by either two RTX Fabs or a single OBZ Fab (Fig. 1B). Cryogenic electron microscopy (cryoEM) imaging of the RTX:CD20 complex allowed us to determine its structure to a resolution of 3.3 Å (fig. S3), resulting in a near-complete atomic model of the complex (Fig. 1C).

The CD20 fold

The RTX:CD20 complex is Y-shaped, with the two RTX Fabs poised on the extracellular face of CD20. CD20 conforms to the predicted 4-transmembrane helix (TM) arrangement, with its 4 TMs arranged anti-parallel and clockwise when viewed from the extracellular side (Fig. 2, top view). The core of each CD20 monomer presents a compacted rectangular-fold measuring ~25 × ~20 × ~50 Å (Fig. 2). Despite low overall sequence identity across the MS4A family (~30%), the structure of CD20 reveals that key structural elements are likely shared by all members (fig. S4A). Most notable is a constellation of highly-conserved, small residues that allow for the close inter-helical packing observed in CD20 and are found along TM1 (Gly53, Gly60, Gly67), TM2 (Gly90, Ser97, Gly98), and TM3 (Ser123, Gly130) (fig. S4A). A set of larger residues contributed by TM2 (Tyr86, Tyr94) and TM4 (Leu194, Met197, Ala201, Gln204) forms the bulk of the tightly-packed TM-helical core (Fig. 2B) and are conserved as similarly-bulky residues in the MS4A family (fig. S4A). Notwithstanding some conformational heterogeneity observed at the intracellular end of TM1, the close interdigitation of highly-conserved residues over ~30 Å creates a tightly sealed 4-TM bundle within the CD20 monomer that is inconsistent with the formation of a transmembrane permeation pathway.

In contrast to the conserved transmembrane core, the extracellular loops (ECLs) of the MS4A family are extremely diverse in sequence (fig. S4A). In CD20, the first extracellular loop (ECL1) is short and largely shielded by ECL2, leaving only Ile76 and Tyr77 exposed (Fig. 2A). The first half of the approximately 35-residue-long ECL2 is an amphipathic sequence that may partially partition into the membrane region and surrounds the perimeter of the 4-helix bundle until it kinks into a single-turn α-helix (Asn153-Arg156), which marks the start of ECL2's extracellular segment (Fig. 2A). Following the α-helix, residues His158 to Ile164 form a circumflex-shaped cap above ECL1, and Ile164 and Tyr165 appear to plug a cavity at the center of the square CD20 fold. The remaining part of ECL2 is stapled by the landmark disulfide bond between Cys167 and Cys183, which is located on an N-terminal extension of helix TM4 (Fig. 2, side view). This region of ECL2, akin to a turret, is by far the most solvent-accessible region of CD20 and contains the known peptide epitope (^{170}ANPSE^{174}) for most anti-CD20 antibodies (*13*).

A search of the protein databank for structures similar to CD20 identified Claudin-3 and CD81 as the nearest matches (*20*, *21*). Although both present similar topologies, structural superposition with CD20 demonstrates poor overall correspondence (fig. S4B). For example, the transmembrane cavity and cholesterol-coordinating acidic residue present in CD81 (*20*) are absent in CD20, and while claudins appear to share a similar core 4-TM packing with CD20, they display a different topology and distinct oligomeric assembly interfaces. We conclude that the three-dimensional structure of CD20 represents a distinct membrane protein fold.

CD20 is a dimer

Previous studies have suggested that CD20 exists as a dimer or a tetramer (*6*–*8*). Viewed from the extracellular side, CD20 forms a dimeric double-barrel assembly of approximate dimensions 20 × 50 Å (Fig. 2, top view). Two square CD20 subunits abut each other to form a four-helix anti-parallel transmembrane coiled-coil involving the upper halves of TM1 (Leu61, Phe62, Ala65, Leu69) and TM4 (Leu189, Ile193, Val196, Phe200) from each protomer (Fig. 2D). The residues at this inter-subunit interface are involved in hydrophobic and van der Waals interactions. In the intracellular half of the transmembrane domain, dimerization is mediated by homotypic contacts between symmetry-related TM1 residues (Thr51, Ala54, Val55, Met58). The close, complementary packing and extensive hydrophobic surface contact at the CD20 dimer interface does not support the existence of an inter-protomer transmembrane conduction pathway. Additionally, structure-based sequence alignment suggests that a CD20-like dimer interface may be shared across the MS4A family (fig. S4A).

The dimeric assembly of CD20 is reinforced by extensive contacts between the extracellular α-helical extension of TM4 and the solvent-exposed region of ECL2. Here, numerous hydrophobic interactions and some polar contacts (Ser179 to Ser179′; Gln181 to backbone amide of Tyr161′) contribute to the interface (Fig. 2C). In total, the CD20 dimer buries 1,656 Å^2 of surface area and has a shape complementarity score of 0.53, comparable to many established dimeric integral membrane proteins [e.g., (*22*, *23*)]. We further examined Tyr182, located near the symmetry axis in CD20, and found that mutation to cysteine (Tyr182Cys) resulted in purification of a covalent dimeric species in the absence of RTX (fig. S1F), consistent with the dimeric assembly observed in our structure. Overall, we conclude that CD20 forms a tight dimeric assembly that places ECL2 loops in close proximity to each other and presents its main epitope (^{170}ANPSE^{174}) in closely associated pairs, less than 20 Å apart.

ECL2 of CD20 is simultaneously recognized by two RTX Fabs

Previous studies have established that the principal epitope of RTX is centered on the ECL2 sequence ^{170}ANPSE^{174} (*13*). In our structure, this core epitope is simultaneously bound by two Fabs, which we denote RTX and RTX′ (Fig. 3). The RTX Fab sits atop the CD20 protomer, engaging ECL2 at a shallow angle (~ 22°) relative to the membrane plane (Fig. 3, side view), likely precluding engagement of CD20 by a single IgG. RTX engulfs the core epitope through numerous van der Waals packing contacts, as well as multiple polar interactions including the hydrogen bond pairs HC.Ser58 – Pro169 (backbone), HC.His35 – Asn171, and HC.Asn33 – Ser173 (backbone and side-chain). The second (RTX′) Fab extends its heavy chain variable loop 3 (H3) across the dimer interface to present HC.Tyr97′, which interacts with Glu174 of CD20 (Fig. 3A). At the apex of ECL2, Ser173 organizes an extended network of hydrogen bonds spanning from HC.Asn33, through Glu174, to HC.Tyr97′ (Fig. 3B). This key interaction network is clamped by both Fabs: Ser173 is stabilized by HC.Tyr52, Glu174 is sandwiched by HC.Trp100b and HC.Gly100′, and HC.Tyr97 is stabilized by HC.Trp100b.

The CD20:RTX complex reveals a distinct secondary epitope

Our structure reveals a second CD20 epitope formed by ECL1 and ECL2 and contacted by complementarity-determining region (CDR) loop L1 of RTX (Fig. 3D). Completely distinct from the classic ECL2 turret epitope ^{170}ANPSE^{174}, this secondary epitope is recognized primarily by light chain residues LC.Ser28, LC.Ser29 and LC.Ser31. Residues LC.Ser28 and LC.Ser29 are positioned to make van der Waals contacts with Ile76 of ECL1 and Pro160 of ECL2, respectively. The side chain of LC.Ser31 is situated atop ECL2's circumflex cap and interfaces with both CD20 protomers: it stabilizes Tyr161 in a CH2-arene-CH2 sandwich also involving Pro160, while its hydroxyl moiety makes van der Waals contacts with Pro178′, which caps the TM4 α-helical extension of the CD20′ protomer. Earlier crystallographic studies of the primary ECL2 turret epitope in complex with RTX had measured a buried surface area of only 440 Å^2 (*4*), but these L1 – ECL1/2 interactions increase the contact surface area by almost 50%, to ~ 640 Å^2 (Fig. 4B), suggesting that this secondary epitope likely contributes significantly to RTX's affinity for CD20.

RTX Fabs are engaged in homotypic contacts

The close proximity (~ 20 Å) of the two primary epitopes displayed by the CD20 dimer results in the RTX Fabs accommodating each other along a homotypic interface between their heavy chains (Fig. 3). CDR loop 3 (H3) dominates the Fab:Fab interface, engaging with its symmetry mate (H3′), and with the H1′ and H2′ loops. Residue HC.Tyr97, which is germline-encoded via the D gene segment (fig. S6A), seems essential to the Fab-Fab interaction: its Cβ and Cγ atoms make close van der Waals contacts with their symmetry mates across the dimer axis, while its aromatic ring stabilizes the backbone of the H3 loop, and its hydroxyl hydrogen-bonds with Glu174′ of the contralateral CD20′ protomer (Fig. 3, A and B). Two key additional Fab:Fab interactions are mediated by HC.Ser31′, whose backbone and side chain directly engage HC.Gly99, while its side chain contacts LC.Tyr49 and HC.Tyr98 (Fig. 3C). Overall, this Fab:Fab homotypic interface buries 375 Å^2 of solvent-exposed area (Fig. 4B).

Our structure has thus unveiled a composite CD20-Fab′ epitope with three components: the primary epitope on ECL2 (^{170}ANPSE^{174}), a secondary ECL1-ECL2 epitope, and a direct

homotypic Fab:Fab interface. The total composite buried surface area of ~ 1,000 Å^2 is comparable to traditional prototypical Fab:protein complexes (*24*), and our observations rationalize how RTX achieves nanomolar affinity for full-length CD20 (table S2) and CD20+ cells (*5*) despite low affinity to the ECL2 epitope peptide (table S3).

RTX's target recognition and CDC activity require the full composite epitope

To ascertain the functional relevance of previously unobserved structural features of the complete CD20 epitope, we introduced targeted mutations into RTX (Fig. 4C). We employed charge reversals and bulky side chains expected to disrupt these molecular interfaces and measured their effects on CDC (Fig. 4E), and on IgG binding to purified CD20 (SPR; table S2), ECL2 epitope peptide (SPR; table S3), and CD20$^+$ cells (flow cytometry; Fig. 4D). For comparison, we included OBZ, which is known to bind cells at levels ~50% lower than RTX and whose Fab can only bind purified CD20 with 1:2 stoichiometry (Fig. 1).

RTX variants LC.Ser28Asp and LC.Ser31Asp were generated to probe the importance of the secondary epitope. Mutation LC.Ser28Asp resulted in reduced CD20 affinity (~20 fold), cellular binding (~ 25%), and CDC activity (IC50 > 10x higher) relative to wild-type RTX. LC.Ser31Asp had a notably stronger phenotype, which resulted in a ~100-fold reduction in Fab:CD20 binding, ~50% reduction in IgG:cell binding, and nearly completely abolished CDC activity. These data substantiate the relevance of this secondary epitope in RTX function.

We next evaluated the role of the germline-encoded HC.Tyr97, because it appears central to complex formation (see above; Fig. 3, A and B). The HC.Tyr97Ser mutation, which we predict may destabilize H3, effectively abolishes target engagement and CDC activity, while mutation HC.Tyr97Phe, which removes only the terminal hydroxyl but maintains the aromaticity of the side chain, reduced affinity to CD20 (~15 fold) as well as cellular binding (~ 25%) and CDC activity (IC50 > 10x higher), suggesting that RTX function is enhanced by the polar interaction between HC.Tyr97 and Glu174′.

To assess the importance of the homotypic Fab:Fab interface, we introduced mutations at HC.Ser31 and HC.Gly99, two positions that are reciprocally involved in interactions at the periphery of the complex. The HC.Ser31Glu mutant had reduced Fab:CD20 affinity (~100-fold), reduced IgG:cell binding and reduced CDC activity (>100-fold). The effect of HC.Gly99Lys was even more marked, with CDC completely abolished. Because these residues are not involved in any interactions with CD20, we conclude that homotypic Fab:Fab interactions potentiate target engagement, cell binding, and CDC activity of RTX.

In summary, we have discovered several RTX mutants that, despite maintaining cell-binding activity comparable to that of OBZ, and largely unaffected binding to the primary ECL2 epitope, are incapable of eliciting CDC. This confirms that the secondary ECL1/2 epitope and Fab:Fab interface contribute to the unique binding properties and high CDC activity of RTX.

Full-length RTX cross-links CD20 dimers into higher-order assemblies

In the RTX Fab:CD20 complex, the distance between the C-termini of the Fab heavy chains (HC.Pro213) is greater than 120 Å, inconsistent with binding of both Fabs from a single IgG to a CD20 dimer (Fig. 1C). This suggests two RTX antibodies engage the dimer, each contributing one of its Fab domains. To test this, we formed complexes in vitro between full-length IgG and CD20 and examined their structural arrangement. We found that these complexes are stable (table S2), and nsEM showed that most CD20 particles were bound by two well-resolved Fabs in a similar geometry to that seen in the CD20:RTX Fab structure (fig. S7G). This establishes that 2:2 complex formation is not exclusive to Fab fragments and occurs readily in the context of full-length RTX.

Unlike OBZ or the RTX Fab, RTX IgG cross-links CD20 into cyclical superstructures of 2-to-2 or 3-to-3 IgGs and CD20s, with approximate diameters of 250 and 300 Å respectively (Fig. 5A). These closed-ring assemblies feature CD20 dimers and Fc domains splayed outwards, linked by pairs of Fab arms which position the Fab-Fc hinges of RTX on a circle of approximate diameter 100 Å (Fig. 5, A and B). Because of the striking similarity with our 3D structure of the CD20:RTX Fab complex, we were able to generate a model of these rings as present on the nsEM grids (Fig. 5, B and C). To understand how these assemblies might relate to RTX function, we endeavored to build a model of an CD20:RTX IgG assembly as it might occur on a cell. This was achieved by rotating each CD20:Fab complex 90 degrees, while keeping the ends of the Fab domains in close proximity to each other (Fig. 5D, left). This modeled assembly exhibits precisely the dimensions that would be required for the three Fc domains to "fold in" (Fig. 5D, middle) and potentially nucleate assembly of a six-membered Fc platform such as those observed in structures of the complement component C1 in complex with Fc (*25*). The resulting model of a CD20:RTX:C1 complex (Fig. 5D, right) provides a structural hypothesis for how Fab:Fab and Fab:CD20 interactions may lay the molecular foundations that promote tight CD20 clustering and complement recruitment, the hallmarks of RTX.

Discussion

CD20 is a clinically-validated target for the treatment of lymphomas and auto-immune diseases, but its structure and

function have remained unknown. In contrast to the prevailing view that CD20 is a tetramer (*13*), our structural studies establish CD20 as a compact dimeric double-barrel assembly, with a protein fold that is distinct from any previously determined structure. Electrostatic surface calculations confirm that the transmembrane helices of CD20 are packed predominantly through hydrophobic and van der Waals complementary interactions. Previous reports have suggested the possibility that CD20 may form a plasma membrane ion channel, but our analyses reveal no plausible ion permeation pathway through the monomeric CD20 protomer or along the dimeric packing interface. We conclude that CD20 and other MS4A family members are unlikely to directly function as ion channels.

The dimeric organization of CD20 finally provides a molecular-level explanation for the perplexing observation that twice as many type I as type II mAbs bind $CD20^{+}$ cells (*17*). Our EM and biophysical studies using purified components establish that each CD20 dimer is bound by two type I RTX Fabs, but only one type II OBZ Fab. The two RTX Fabs are brought in close proximity due to CD20's compact symmetrical dimeric arrangement, resulting in an extensive homotypic Fab:Fab interface, which necessitates a shallow angle of approach of the Fabs. This orientation avoids steric clashes between the two RTX Fabs, whereas OBZ's steeper angle of approach (*5*) would be expected to sterically preclude another Fab from binding.

Though it has long been known that RTX promotes CD20 clustering on the cell surface, our observation of circular RTX:CD20 assemblies with a diameter similar to that required for Fc hexamer formation (Fig. 5, A and B) raises the possibility that RTX-induced cell-surface CD20 clusters may in fact be well-ordered assemblies specifically predisposed to recruit complement (as opposed to loose groupings on the cell surface). Assemblies of this kind could be particularly efficient at complement recruitment by virtue of their biasing of Fc domain positions and orientations toward the formation of the hexameric Fc platforms necessary for complement recruitment (*25*). In a simplistic model, we speculate that dimeric RTX:CD20 building blocks (Fig. 1C) can assemble into a 3-to-3 closed-ring configuration that acts as a nucleating scaffold for IgG hexamer formation to ultimately recruit C1q (Fig. 5D). One unknown or caveat in this model is that it requires the recruitment of three additional RTX IgG molecules that are not involved in the initial 3-to-3 ring but are needed to achieve Fc hexamerization. Once formed, it seems plausible that 3-to-3 ring assemblies could serve to potentiate Fc-Fc interactions by intermingling with various other RTX:CD20 superstructures (Fig. 5A) or assembly intermediates that are likely found and enriched along the cell surface, ultimately leading to efficient Fc-hexamer formation and C1q engagement. Although further experiments are needed to ascertain the precise dynamics and geometrical arrangements of RTX:CD20 complexes on the cell membrane when IgG hexamers are formed, our proposed model for C1q recruitment by RTX (Fig. 5D) provides an initial molecular-level hypothesis for why type I mAbs elicit potent CDC. This speculative structure-based model also suggests that CDC functionality may be shared more generally by antibodies which bind oligomeric cell-surface targets and leave at least one epitope unencumbered and available for further mAb binding.

In the case of RTX, the simultaneous binding of both CD20 subunits is made possible by an intricate geometrical arrangement involving Fab:CD20 contacts at a secondary epitope and a large Fab:Fab interaction surface. We note that all of the RTX residues involved in this homotypic interaction are germline encoded in mice (fig. S6A). This observation suggests that the homotypic Fab:Fab interaction was inherent to the progenitor RTX B cell prior to somatic hypermutation. These residues are also highly conserved among the RTX-like type I mAbs (fig. S6B), a majority of which are also mouse-derived. Similar Fab:Fab contacts mediate crystal-packing of the isolated RTX Fab-ECL2 peptide complex (*4*) (fig. S5), which, taken together with our findings, indicates that Fab-Fab homotypic interactions are energetically favorable and an essential feature of the RTX-like type I mAbs. This raises the question of whether RTX Fabs may exist as pre-formed dimers prior to CD20 binding. We evaluated this possibility but found only weak Fab:Fab interactions at extremely high concentrations (>100 μM; data not shown), suggesting that the homotypic Fab:Fab interactions are nucleated by CD20 binding. We are aware of two other examples of Fab:Fab homotypic interaction, and in each case, these interfaces are central to antibody function: neutralization of a malaria parasite (*26*, *27*), and cross-linking-independent activation of TRAIL-R2 (*28*). Given the functional relevance of homotypic Fab:Fab interfaces in these three exemplar cases, we propose that these observations can be exploited in the discovery and optimization of next-generation therapeutic antibodies.

REFERENCES AND NOTES

1. M. J. E. Marshall, R. J. Stopforth, M. S. Cragg, Therapeutic antibodies: What have we learnt from targeting CD20 and where are we going? *Front. Immunol.* **8**, 1245 (2017). doi:10.3389/fimmu.2017.01245 Medline
2. P. Stashenko, L. M. Nadler, R. Hardy, S. F. Schlossman, Characterization of a human B lymphocyte-specific antigen. *J. Immunol.* **125**, 1678–1685 (1980). Medline
3. L. Eon Kuek, M. Leffler, G. A. Mackay, M. D. Hulett, The MS4A family: Counting past 1, 2 and 3. *Immunol. Cell Biol.* **94**, 11–23 (2016). doi:10.1038/icb.2015.48 Medline
4. J. Du, H. Wang, C. Zhong, B. Peng, M. Zhang, B. Li, S. Huo, Y. Guo, J. Ding, Structural basis for recognition of CD20 by therapeutic antibody rituximab. *J. Biol. Chem.* **282**, 15073–15080 (2007). doi:10.1074/jbc.M701654200 Medline
5. G. Niederfellner, A. Lammens, O. Mundigl, G. J. Georges, W. Schaefer, M. Schwaiger, A. Franke, K. Wiechmann, S. Jenewein, J. W. Slootstra, P. Timmerman, A. Brännström, F. Lindstrom, E. Mössner, P. Umana, K.-P. Hopfner, C. Klein, Epitope characterization and crystal structure of GA101 provide insights into the molecular basis for type I/II distinction of CD20 antibodies. *Blood* **118**, 358–367 (2011). doi:10.1182/blood-2010-09-305847 Medline

6. J. K. Bubien, L. J. Zhou, P. D. Bell, R. A. Frizzell, T. F. Tedder, Transfection of the CD20 cell surface molecule into ectopic cell types generates a Ca^{2+} conductance found constitutively in B lymphocytes. *J. Cell Biol.* **121**, 1121–1132 (1993). doi:10.1083/jcb.121.5.1121 Medline
7. M. J. Polyak, J. P. Deans, Alanine-170 and proline-172 are critical determinants for extracellular CD20 epitopes; heterogeneity in the fine specificity of CD20 monoclonal antibodies is defined by additional requirements imposed by both amino acid sequence and quaternary structure. *Blood* **99**, 3256–3262 (2002). doi:10.1182/blood.V99.9.3256 Medline
8. M. J. Polyak, H. Li, N. Shariat, J. P. Deans, CD20 homo-oligomers physically associate with the B cell antigen receptor. Dissociation upon receptor engagement and recruitment of phosphoproteins and calmodulin-binding proteins. *J. Biol. Chem.* **283**, 18545–18552 (2008). doi:10.1074/jbc.M800784200 Medline
9. T. W. Kuijpers, R. J. Bende, P. A. Baars, A. Grummels, I. A. M. Derks, K. M. Dolman, T. Beaumont, T. F. Tedder, C. J. M. van Noesel, E. Eldering, R. A. W. van Lier, CD20 deficiency in humans results in impaired T cell-independent antibody responses. *J. Clin. Invest.* **120**, 214–222 (2010). doi:10.1172/JCI40231 Medline
10. C. A. Walshe, S. A. Beers, R. R. French, C. H. T. Chan, P. W. Johnson, G. K. Packham, M. J. Glennie, M. S. Cragg, Induction of cytosolic calcium flux by CD20 is dependent upon B cell antigen receptor signaling. *J. Biol. Chem.* **283**, 16971–16984 (2008). doi:10.1074/jbc.M708459200 Medline
11. D. G. Maloney, A. J. Grillo-López, C. A. White, D. Bodkin, R. J. Schilder, J. A. Neidhart, N. Janakiraman, K. A. Foon, T.-M. Liles, B. K. Dallaire, K. Wey, I. Royston, T. Davis, R. Levy, IDEC-C2B8 (rituximab) anti-CD20 monoclonal antibody therapy in patients with relapsed low-grade non-Hodgkin's lymphoma. *Blood* **90**, 2188–2195 (1997). doi:10.1182/blood.V90.6.2188 Medline
12. X. Montalban, S. L. Hauser, L. Kappos, D. L. Arnold, A. Bar-Or, G. Comi, J. de Seze, G. Giovannoni, H.-P. Hartung, B. Hemmer, F. Lublin, K. W. Rammohan, K. Selmaj, A. Traboulsee, A. Sauter, D. Masterman, P. Fontoura, S. Belachew, H. Garren, N. Mairon, P. Chin, J. S. Wolinsky; ORATORIO Clinical Investigators, Ocrelizumab versus placebo in primary progressive multiple sclerosis. *N. Engl. J. Med.* **376**, 209–220 (2017). doi:10.1056/NEJMoa1606468 Medline
13. C. Klein, A. Lammens, W. Schäfer, G. Georges, M. Schwaiger, E. Mössner, K.-P. Hopfner, P. Umaña, G. Niederfellner, Epitope interactions of monoclonal antibodies targeting CD20 and their relationship to functional properties. *MAbs* **5**, 22–33 (2013). doi:10.4161/mabs.22771 Medline
14. J. P. Deans, S. M. Robbins, M. J. Polyak, J. A. Savage, Rapid redistribution of CD20 to a low density detergent-insoluble membrane compartment. *J. Biol. Chem.* **273**, 344–348 (1998). doi:10.1074/jbc.273.1.344 Medline
15. W. G. Wierda, T. J. Kipps, J. Mayer, S. Stilgenbauer, C. D. Williams, A. Hellmann, T. Robak, R. R. Furman, P. Hillmen, M. Trneny, M. J. S. Dyer, S. Padmanabhan, M. Piotrowska, T. Kozak, G. Chan, R. Davis, N. Losic, J. Wilms, C. A. Russell, A. Österborg; Hx-CD20-406 Study Investigators, Ofatumumab as single-agent CD20 immunotherapy in fludarabine-refractory chronic lymphocytic leukemia. *J. Clin. Oncol.* **28**, 1749–1755 (2010). doi:10.1200/JCO.2009.25.3187 Medline
16. E. Mössner, P. Brünker, S. Moser, U. Püntener, C. Schmidt, S. Herter, R. Grau, C. Gerdes, A. Nopora, E. van Puijenbroek, C. Ferrara, P. Sondermann, C. Jäger, P. Strein, G. Fertig, T. Friess, C. Schüll, S. Bauer, J. Dal Porto, C. Del Nagro, K. Dabbagh, M. J. S. Dyer, S. Poppema, C. Klein, P. Umaña, Increasing the efficacy of CD20 antibody therapy through the engineering of a new type II anti-CD20 antibody with enhanced direct and immune effector cell-mediated B-cell cytotoxicity. *Blood* **115**, 4393–4402 (2010). doi:10.1182/blood-2009-06-225979 Medline
17. H. T. C. Chan, D. Hughes, R. R. French, A. L. Tutt, C. A. Walshe, J. L. Teeling, M. J. Glennie, M. S. Cragg, CD20-induced lymphoma cell death is independent of both caspases and its redistribution into triton X-100 insoluble membrane rafts. *Cancer Res.* **63**, 5480–5489 (2003). Medline
18. J. Du, H. Yang, Y. Guo, J. Ding, Structure of the Fab fragment of therapeutic antibody Ofatumumab provides insights into the recognition mechanism with CD20. *Mol. Immunol.* **46**, 2419–2423 (2009). doi:10.1016/j.molimm.2009.04.009 Medline
19. J. Du, H. Wang, C. Zhong, B. Peng, M. Zhang, B. Li, S. Hou, Y. Guo, J. Ding, Crystal structure of chimeric antibody C2H7 Fab in complex with a CD20 peptide. *Mol. Immunol.* **45**, 2861–2868 (2008). doi:10.1016/j.molimm.2008.01.034 Medline
20. B. Zimmerman, B. Kelly, B. J. McMillan, T. C. M. Seegar, R. O. Dror, A. C. Kruse, S. C. Blacklow, Crystal structure of a full-length human tetraspanin reveals a cholesterol-binding pocket. *Cell* **167**, 1041–1051.e11 (2016). doi:10.1016/j.cell.2016.09.056 Medline
21. S. Nakamura, K. Irie, H. Tanaka, K. Nishikawa, H. Suzuki, Y. Saitoh, A. Tamura, S. Tsukita, Y. Fujiyoshi, Morphologic determinant of tight junctions revealed by claudin-3 structures. *Nat. Commun.* **10**, 816 (2019). doi:10.1038/s41467-019-08760-7 Medline
22. R. Dutzler, E. B. Campbell, M. Cadene, B. T. Chait, R. MacKinnon, X-ray structure of a ClC chloride channel at 3.0 Å reveals the molecular basis of anion selectivity. *Nature* **415**, 287–294 (2002). doi:10.1038/415287a Medline
23. F. Li, J. Liu, Y. Zheng, R. M. Garavito, S. Ferguson-Miller, Crystal structures of translocator protein (TSPO) and mutant mimic of a human polymorphism. *Science* **347**, 555–558 (2015). doi:10.1126/science.1260590 Medline
24. T. Ramaraj, T. Angel, E. A. Dratz, A. J. Jesaitis, B. Mumey, Antigen-antibody interface properties: Composition, residue interactions, and features of 53 non-redundant structures. *Biochim. Biophys. Acta.* **1824**, 520–532 (2012). doi:10.1016/j.bbapap.2011.12.007 Medline
25. D. Ugurlar, S. C. Howes, B.-J. de Kreuk, R. I. Koning, R. N. de Jong, F. J. Beurskens, J. Schuurman, A. J. Koster, T. H. Sharp, P. W. H. I. Parren, P. Gros, Structures of C1-IgG1 provide insights into how danger pattern recognition activates complement. *Science* **359**, 794–797 (2018). doi:10.1126/science.aao4988 Medline
26. K. Imkeller, S. W. Scally, A. Bosch, G. P. Martí, G. Costa, G. Triller, R. Murugan, V. Renna, H. Jumaa, P. G. Kremsner, B. K. L. Sim, S. L. Hoffman, B. Mordmüller, E. A. Levashina, J.-P. Julien, H. Wardemann, Antihomotypic affinity maturation improves human B cell responses against a repetitive epitope. *Science* **360**, 1358–1362 (2018). doi:10.1126/science.aar5304 Medline
27. D. Oyen, J. L. Torres, C. A. Cottrell, C. Richter King, I. A. Wilson, A. B. Ward, Cryo-EM structure of *P. falciparum* circumsporozoite protein with a vaccine-elicited antibody is stabilized by somatically mutated inter-Fab contacts. *Sci. Adv.* **4**, eaau8529 (2018). doi:10.1126/sciadv.aau8529 Medline
28. T. Tamada, D. Shinmi, M. Ikeda, Y. Yonezawa, S. Kataoka, R. Kuroki, E. Mori, K. Motoki, TRAIL-R2 superoligomerization induced by human monoclonal agonistic antibody KMTR2. *Sci. Rep.* **5**, 17936 (2015). doi:10.1038/srep17936 Medline
29. L. C. Simmons, D. Reilly, L. Klimowski, T. S. Raju, G. Meng, P. Sims, K. Hong, R. L. Shields, L. A. Damico, P. Rancatore, D. G. Yansura, Expression of full-length immunoglobulins in *Escherichia coli*: Rapid and efficient production of aglycosylated antibodies. *J. Immunol. Methods* **263**, 133–147 (2002). doi:10.1016/S0022-1759(02)00036-4 Medline
30. G. B. Fields, R. L. Noble, Solid phase peptide synthesis utilizing 9-fluorenylmethoxycarbonyl amino acids. *Int. J. Pept. Protein Res.* **35**, 161–214 (1990). doi:10.1111/j.1399-3011.1990.tb00939.x Medline
31. T. Grant, A. Rohou, N. Grigorieff, *cis*TEM, user-friendly software for single-particle image processing. *eLife* **7**, e35383 (2018). doi:10.7554/eLife.35383 Medline
32. D. N. Mastronarde, Automated electron microscope tomography using robust prediction of specimen movements. *J. Struct. Biol.* **152**, 36–51 (2005). doi:10.1016/j.jsb.2005.07.007 Medline
33. P. Emsley, B. Lohkamp, W. G. Scott, K. Cowtan, Features and development of *Coot*. *Acta Crystallogr. Sect. D Biol. Crystallogr.* **66**, 486–501 (2010). doi:10.1107/S0907444910007493 Medline
34. T. I. Croll, *ISOLDE*: A physically realistic environment for model building into low-resolution electron-density maps. *Acta Crystallogr. Sect. D Struct. Biol.* **74**, 519–530 (2018). doi:10.1107/S2059798318002425 Medline
35. P. V. Afonine, B. K. Poon, R. J. Read, O. V. Sobolev, T. C. Terwilliger, A. Urzhumtsev, P. D. Adams, Real-space refinement in *PHENIX* for cryo-EM and crystallography. *Acta Crystallogr. Sect. D Struct. Biol.* **74**, 531–544 (2018). doi:10.1107/S2059798318006551 Medline
36. R. Norel, S. L. Lin, H. J. Wolfson, R. Nussinov, Shape complementarity at protein-protein interfaces. *Biopolymers* **34**, 933–940 (1994). doi:10.1002/bip.360340711 Medline
37. T. D. Goddard, C. C. Huang, E. C. Meng, E. F. Pettersen, G. S. Couch, J. H. Morris, T. E. Ferrin, UCSF ChimeraX: Meeting modern challenges in visualization and analysis. *Protein Sci.* **27**, 14–25 (2018). doi:10.1002/pro.3235 Medline
38. L. Holm, Benchmarking fold detection by DaliLite v.5. *Bioinformatics* **35**, 5326–

5327 (2019). doi:10.1093/bioinformatics/btz536 Medline
39. F. Madeira, Y. M. Park, J. Lee, N. Buso, T. Gur, N. Madhusoodanan, P. Basutkar, A. R. N. Tivey, S. C. Potter, R. D. Finn, R. Lopez, The EMBL-EBI search and sequence analysis tools APIs in 2019. *Nucleic Acids Res.* **47**, W636–W641 (2019). doi:10.1093/nar/gkz268 Medline
40. G. Cardone, J. B. Heymann, A. C. Steven, One number does not fit all: Mapping local variations in resolution in cryo-EM reconstructions. *J. Struct. Biol.* **184**, 226–236 (2013). doi:10.1016/j.jsb.2013.08.002 Medline

ACKNOWLEDGMENTS

Molecular graphics and analyses performed with UCSF ChimeraX, developed by the Resource for Biocomputing, Visualization, and Informatics at the University of California, San Francisco, with support from NIH R01-GM129325 and P41-GM103311. Thanks to the entire Biomolecular resources (BMR) department at Genentech for support throughout the project. Thanks to the Peptide Synthesis group in the department of Early Discovery Biochemistry at Genentech. We thank the Research Material Group (RMG) for antibody expression as well as the Wu lab in Protein Chemistry and the Antibody Production and Automation Technologies group for antibody purification. **Funding:** T.C. was supported by a Principal Research Fellowship from the Wellcome Trust to Randy Read (grant number 209407/Z/17/Z) and gratefully acknowledges the support of NVIDIA Corporation with the donation of the Titan Xp GPU used for this research. All other authors are employees of Genentech, Inc. **Author contributions:** Project conceptualization: C.Ko., A.R.; CD20 construct design: C.Ko., L.R.; CD20 protein production: C.Ku., C.T., E.K.; Electron microscopy: A.E., C.A., C.C.; EM image processing: L.R., A.R.; Model building and refinement: A.R., T.C.; Structure analysis: A.R., J.P., J.T.K., L.R.; Antibody protein production, flow cytometry and CDC assays: N.C., G.N.; Antibody mutant design and selection: A.R., J.T.K., G.N., L.R.; Manuscript writing: A.R., J.P., J.T.K.; SPR: M.S.; CD20 purification, EM sample preparation, BLI, DSF, SEC-MALS: L.R.; J.P., G.N., J.T.K. and A.R. are co-senior authors; A.R. supervised the project. **Competing interests:** All authors except T.C. are employees of Genentech, Inc. **Data and materials availability:** Materials will be made available upon request and material transfer agreement with Genentech. Accession numbers of the CD20:RTX Fab model and map are PDB 6VJA and EMD-21212, respectively.

SUPPLEMENTARY MATERIALS

science.sciencemag.org/cgi/content/full/science.aaz9356/DC1
Materials and Methods
Figs. S1 to S7
Tables S1 to S4
References (*29–40*)

29 October 2019; accepted 6 February 2020
Published online 20 February 2020
10.1126/science.aaz9356

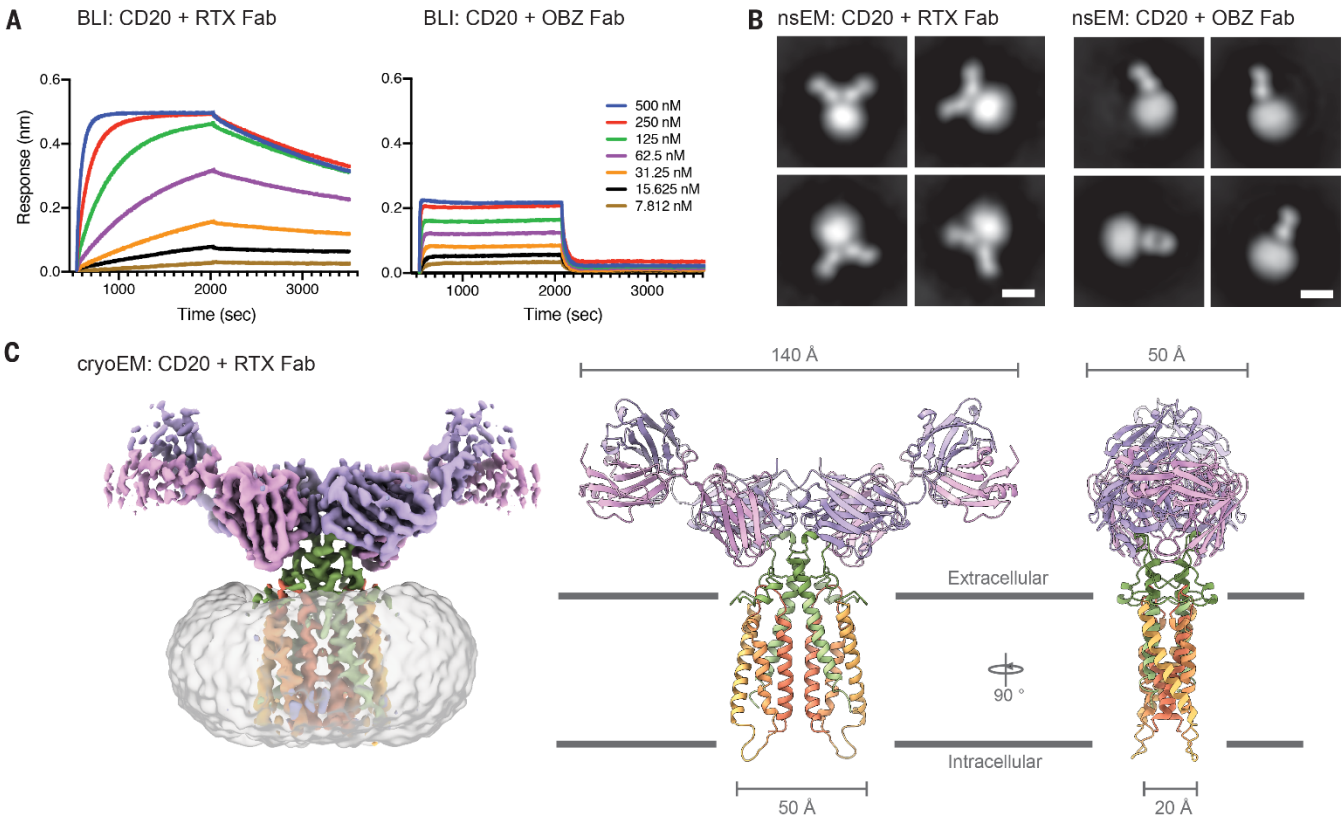

Fig. 1. Characterization of CD20:Fab complexes and cryoEM structure of CD20:RTX Fab. (**A**) Biolayer interferometry (BLI) traces. A serial dilution of RTX (left) or OBZ (right) Fabs was flowed in for the first 1,500 s of the experiments, followed by a dissociation step. (**B**) Negative-stain EM (nsEM) of expressed, solubilized and purified CD20 in complex with RTX (left) or OBZ (right) Fab. Scale bar: 50 Å. (**C**) CryoEM reconstruction of the CD20:RTX Fab complex, at a resolution of 3.3 Å. Left panel: isosurface rendering, with the GDN micelle rendered in transparent grey, the RTX Fab heavy chain in purple and the light chain in pink. Right panel: two orthogonal side views (along the plane of the membrane) of a ribbon rendering of the structure.

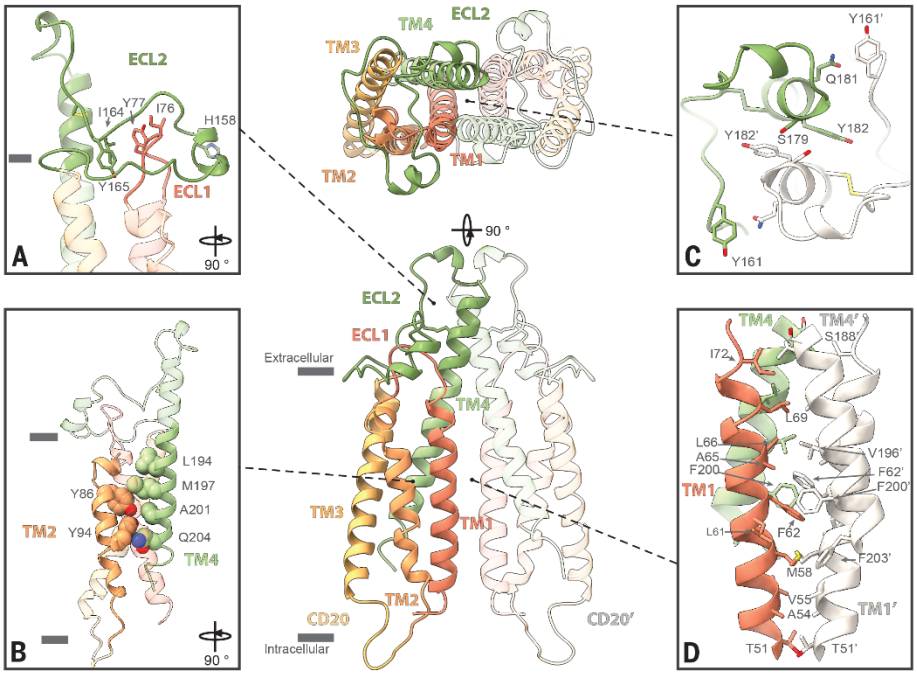

Fig. 2. The CD20 dimer is a compact double square-barrel structure. Ribbon diagrams of the CD20 structure, with RTX omitted and one of the CD20 protomers transparent, for clarity. (**A**) The short loop ECL1 (red), between TM1 and TM2, is almost entirely surrounded by the first half of ECL2 (green). (**B**) The core of each protomer is marked by a number of highly-conserved small (mostly glycine) residues (not shown) and a complementary set of bulkier residues shown here in space-filling representation. (**C** and **D**) The extensive dimeric interface of CD20 involves the extracellular domain (C) as well as TM helices 1 and 4 (D).

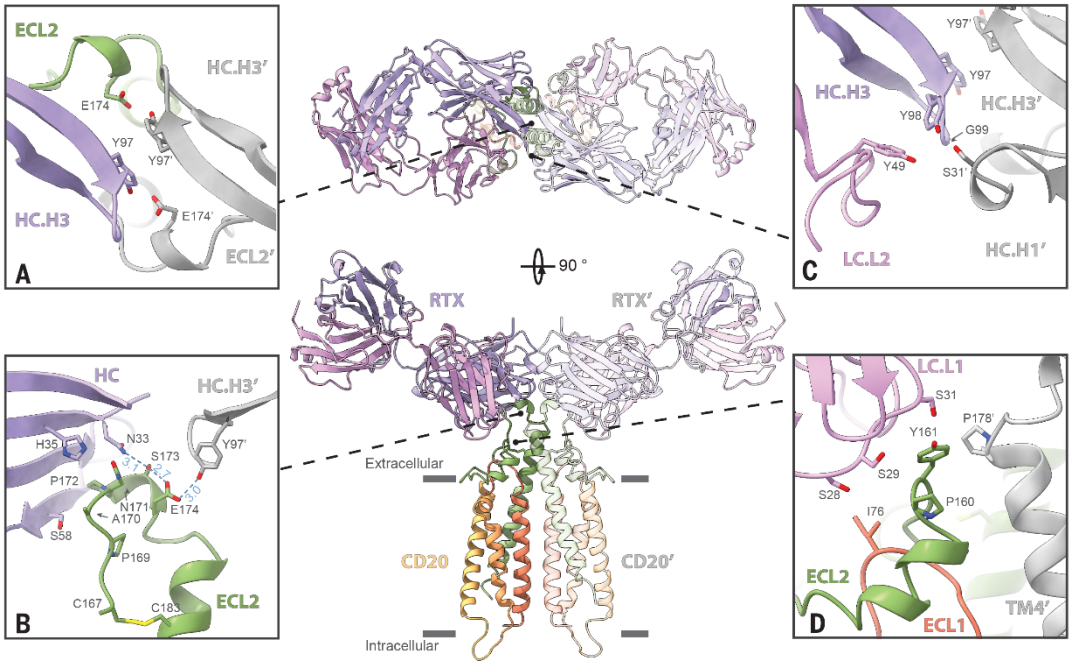

Fig. 3. Key molecular interactions between CD20 and RTX. Ribbon diagrams of the CD20:RTX Fab structure, with key amino acid side chains involved in CD20:RTX or RTX:RTX shown in stick representation. (**A**) Top view of the center of the complex, where HC.Tyr97 mediates Fab:Fab and Fab:CD20′ contacts. (**B**) The canonical RTX epitope ^{170}ANPSE^{174}, in addition to being recognized by RTX's heavy chain (left, purple), is also involved in a hydrogen bond network with Tyr97′ from the distal RTX Fab (right, grey). (**C**) Additional Fab:Fab contacts between heavy chain (HC) loops H3 and H1 and light chain (LC) loop L2. (**D**) A secondary epitope consisting of ECL1 and ECL2 is contacted by RTX's LC loop 1.

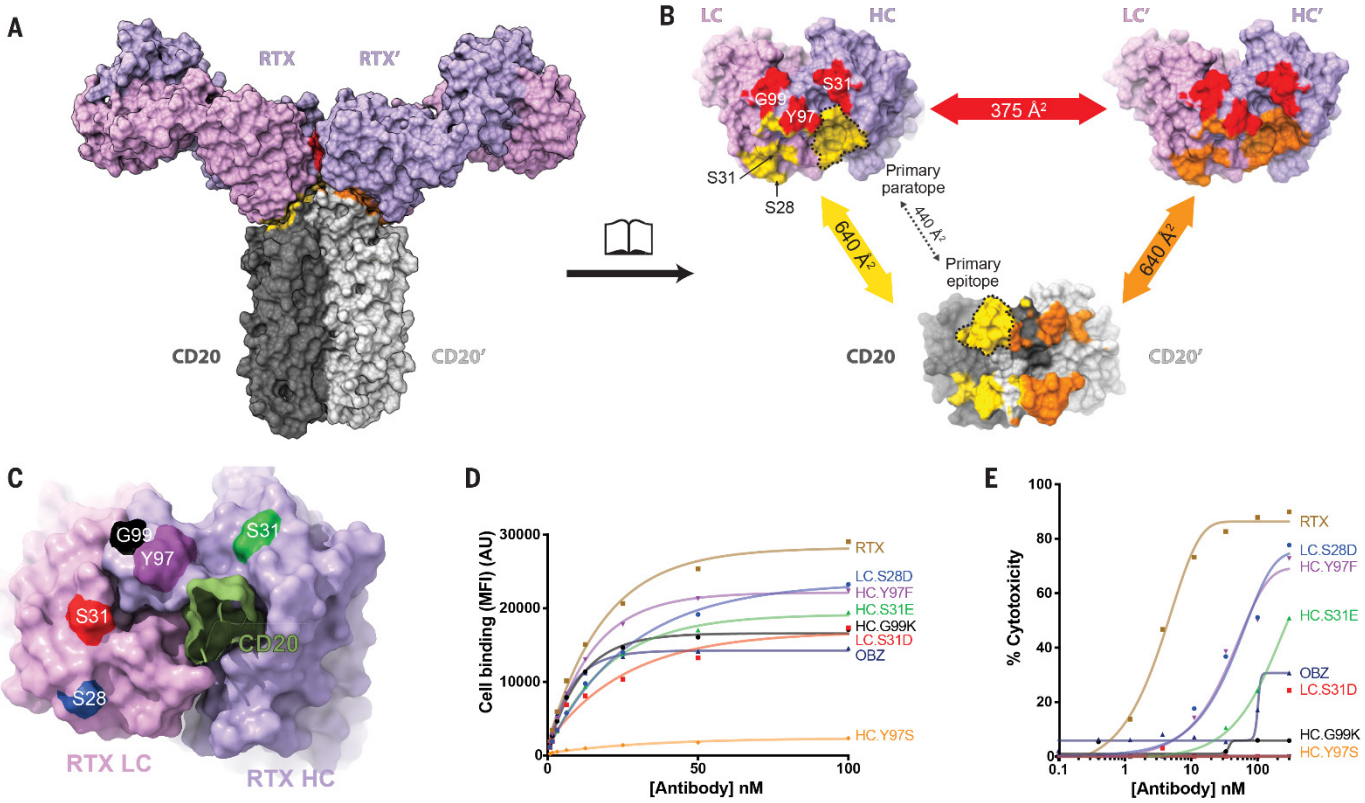

Fig. 4. Multiple CD20:RTX and RTX:RTX interactions enable cell binding and CDC. (**A**) Surface representation of the CD20:RTX Fab complex. The surfaces buried by complex formation are colored in yellow (CD20:RTX), orange (CD20′:RTX′), or red (RTX:RTX′). (**B**) Open-book representation of the same surfaces, with surface area measurements for each buried surface indicated. Residues mutated as part of this study are labeled in the top left panel and are not involved in the primary paratope. The primary epitope (dashed line) only accounts for less than half (440 Å^2 out of 1,015 Å^2) of the total Fab binding area. (**C**) Surface representation of the CDR face of RTX Fab, with the ECL2 turret epitope shown (green), as well as the positions of the point mutations under study. (**D** and **E**) Complement-dependent cytotoxicity (D) and cell binding (E) of RTX mutants are plotted as a function of antibody concentration, and compared to wild-type RTX and OBZ.

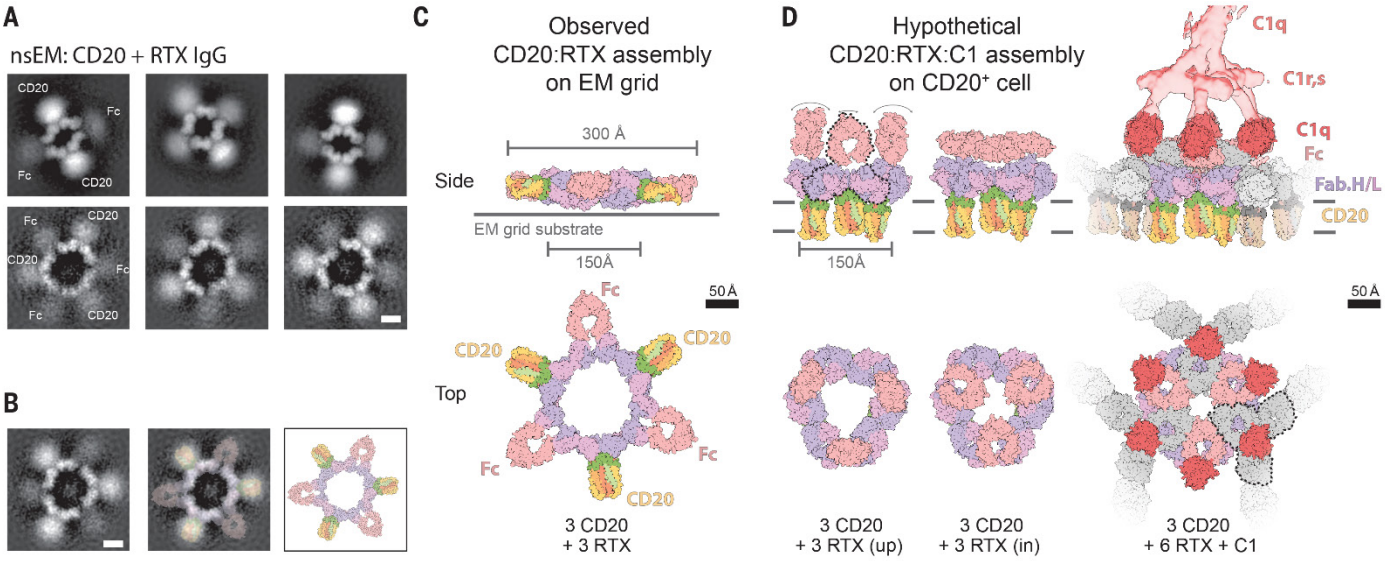

Fig. 5. RTX cross-links CD20 into circular super-assemblies. (**A**) Average nsEM images of CD20 incubated with full-length RTX show cyclical higher-order structures of involving 2-to-2 (top row; diameter of 250 Å) or 3-to-3 (bottom row; diameter of 300 Å) CD20-to-RTX complexes. The RTX Fc domains appear disordered, presumably because of IgG hinge flexibility. (**B** and **C**) Interpretation of an nsEM class average of a 3-to-3 assembly. (**D**) Proposed model for CD20:RTX super-complex formation and complement recruitment. During nsEM experiments, the IgGs and solubilized CD20s are co-planar (C). Modeling these high-order assemblies as they might occur at the surface of CD20⁺ cells requires rotating the CD20:Fab complexes 90 degrees [(D), left]. Given the flexibility provided by the IgG hinges, it is then possible to position Fc domains (pink) in a common plane [(D), middle]. The addition of three further Fc domains possibly contributed by neighboring CD20:IgG assemblies (grey) would complete the Fc hexamer formation and enable recruitment of C1q [(D), right]. Dashed lines outline IgG molecules. Models used: structure from present work (RTX Fab:CD20 complex), EMDB-4232 (EM map of C1:Fc complex) and PDB 6FCZ (Fc domains and C1q head domains) (*25*).

Structure of CD20 in complex with the therapeutic monoclonal antibody rituximab

Lionel Rougé, Nancy Chiang, Micah Steffek, Christine Kugel, Tristan I. Croll, Christine Tam, Alberto Estevez, Christopher P. Arthur, Christopher M. Koth, Claudio Ciferri, Edward Kraft, Jian Payandeh, Gerald Nakamura, James T. Koerber and Alexis Rohou

published online February 20, 2020